Am J Physiol Cell Physiol 304: C1013–C1026, 2013.
First published March 13, 2013; doi:10.1152/ajpcell.00254.2012.

On the role of ATP release, ectoATPase activity, and extracellular ADP in the regulatory volume decrease of Huh-7 human hepatoma cells

María V. Espelt,[1] Felicitas de Tezanos Pinto,[1] Cora L. Alvarez,[1] Germán Sanchez Alberti,[1] Jeremías Incicco,[1] María F. Leal Denis,[1] Carlos Davio,[2] and Pablo J. Schwarzbaum[1]

[1]*Instituto de Química y Fisicoquímica Biológicas (Facultad de Farmacia y Bioquímica), Universidad de Buenos Aires, Buenos Aires, Argentina; and* [2]*Departamento de Farmacología (Facultad de Farmacia y Bioquímica), Universidad de Buenos Aires, Buenos Aires, Argentina*

Submitted 30 July 2012; accepted in final form 12 March 2013

Espelt MV, de Tezanos Pinto F, Alvarez CL, Alberti GS, Incicco J, Denis MF, Davio C, Schwarzbaum PJ. On the role of ATP release, ectoATPase activity, and extracellular ADP in the regulatory volume decrease of Huh-7 human hepatoma cells. *Am J Physiol Cell Physiol* 304: C1013–C1026, 2013. First published March 13, 2013; doi:10.1152/ajpcell.00254.2012.—Hypotonicity triggered in human hepatoma cells (Huh-7) the release of ATP and cell swelling, followed by volume regulatory decrease (RVD). We analyzed how the interaction between those processes modulates cell volume. Cells exposed to hypotonic medium swelled 1.5 times their basal volume. Swelling was followed by 41% RVD_{40} (extent of RVD after 40 min of maximum), whereas the concentration of extracellular ATP (ATP_e) increased 10 times to a maximum value at 15 min. Exogenous apyrase (which removes di- and trinucleotides) did not alter RVD, whereas exogenous Na^+-K^+-ATPase (which converts ATP to ADP in the extracellular medium) enhanced RVD_{40} by 2.6 times, suggesting that hypotonic treatment alone produced a basal RVD, whereas extracellular ADP activated RVD to achieve complete volume regulation (i.e., $RVD_{40} \approx 100\%$). Under hypotonicity, addition of 2-(methylthio)adenosine 5′-diphosphate (2MetSADP; ADP analog) increased RVD to the same extent as exposure to Na^+-K^+-ATPase and the same analog did not stimulate RVD when coincubated with MRS2211, a blocker of ADP receptor $P2Y_{13}$. RT-PCR and Western blot analysis confirmed the presence of $P2Y_{13}$. Cells exhibited significant ectoATPase activity, which according to RT-PCR analysis can be assigned to ENTPDase2. Both carbenoxolone, a blocker of conductive ATP release, and brefeldin A, an inhibitor of exocytosis, were able to partially decrease ATP_e accumulation, pointing to the presence of at least two mechanisms for ATP release. Thus, in Huh-7 cells, hypotonic treatment triggered the release of ATP. Conversion of ATP_e to ADP_e by ENTPDase 2 activity facilitates the accumulated ADP_e to activate $P2Y_{13}$ receptors, which mediate complete RVD.

cell volume regulation; human hepatoma; nucleotides; $P2Y_{13}$ receptor; purinergic signaling

IN MOST ANIMAL CELLS, A REDUCTION of extracellular osmolarity or an increase in intracellular osmolarity leads to a net influx of water causing volume increase. Not surprisingly, cells exhibit volume regulatory mechanisms that prevent excessive swelling leading to cell bursting and excessive shrinkage that would compromise proper cell metabolism (24). Cell swelling is followed by a slower recovery towards the preshock level, a process known as regulatory volume decrease (RVD; Refs. 27, 38). This response is mediated to a large extent by the efflux of intracellular osmolytes, thereby generating a driving force for water efflux. Swollen cells of liver and hepatoma cells lose Cl^- and K^+ through electroneutral ion transport pathways or by the separate activation of K^+ and anion channels (27).

Although many intracellular signaling processes of cell volume regulation are now well characterized (29), comparatively little is known regarding the extracellular factors controlling RVD (14, 48, 49). In this respect, mechanical stimuli such as shear stress (7), mechanical strain (55), and hypotonic stress (45) have been shown to induce the release of ATP in the absence of lysis from a variety of cells (36, 44, 51, 52, 61), whereas addition of exogenous ATP to hypotonic cells suspensions was able to stimulate RVD (32, 49). In principle ATP can be released both by a conductive channel-mediated pathway, driven by the steep electrochemical gradient of ATP through the plasma membrane, and by vesicular transport via exocytosis (19, 22, 23, 40). In liver cells, increases in cell volume of both cholangiocytes and human cholangiocarcinoma trigger parallel changes in vesicular exocytosis and ATP release, whereas in rat hepatoma cells intracellular ATP is localized in discrete vesicles originated from a bafilomycin A1-sensitive pool that are depleted by hypotonic exposure, thus implying an important role of exocytosis in regulated release of ATP from hepatic cells (22).

Examples of ATP-induced volume regulation were observed in hepatocytes, hepatoma (21, 23, 61), endothelial cells, astrocytes, and epithelial cells from human and several other mammalian species (6, 7, 36). Similarly, swollen cells could be induced to downregulate their volume in the presence of nucleotides other than ATP, such as UTP, UDP, or ATPγS (but not ADP) in fish hepatocytes (9, 10 17, 49), and UTP in salivary gland duct cells (33).

In general, the action of extracellular ATP (ATP_e) and other nucleotides on RVD requires the activation of cell surface purinergic receptors called P2 (type 2 receptors for purinic and pyrimidinic di- and trinucleotides; Ref. 39). The P2 receptor family (12) consists of two main subtypes, P2X and P2Y, representing ligand-gated cation channels and G protein-coupled receptors, respectively. Whereas P2X receptors respond only to ATP, P2Y receptors can be activated by ATP, ADP, UTP, UDP, ITP, and nucleotide sugars, although specificity varies among subtypes (1). Activation of some P2 receptor subtypes ($P2Y_2$, $P2Y_4$, $P2Y_6$, and $P2Y_{11}$) is coupled to increases in intracellular Ca^{2+} (via activation of G_q/G_{11} protein), while other subtypes (P2Y1, $P2Y_{12}$, $P2Y_{13}$, and $P2Y_{14}$) triggered increases in intracellular cAMP (via G_i/G_o protein; Ref. 1).

Address for reprint requests and other correspondence: M. V. Espelt, Instituto de Química y Fisicoquímica Biológicas (Facultad de Farmacia y Bioquímica), Universidad de Buenos Aires, Buenos Aires, Argentina (e-mail: victoria@qb.ffyb.uba.ar).

In rat hepatoma cells and human hepatocytes, ATP_e couples increases in cell volume to stimulation of Cl^- permeability via activation of specific P2Y receptors subtypes (21, 53, 61).

In spite of the accumulated knowledge showing how activation of P2 receptors by extracellular nucleotides regulates the permeability of osmolytes and cell volume, the role of extracellular metabolism of these nucleotides on the RVD response remained largely unexplored. This is important since signaling of specific P2 receptor subtypes modulating the RVD will depend on the time-dependent changes in the concentrations of nucleotides and its hydrolysis products on the cell surface.

Accordingly, ATP can be metabolized extracellularly by a family of ectonucleotidases that restrain the action of ATP_e on certain P receptors, while at the same time generate different byproducts (notably ADP and adenosine) that can accumulate at the cell surface and signal, autocrinally and paracrinally, via specific P receptors subtypes. In many tissues and cells, members of the ectonucleoside triphosphate diphosphohydrolase (ENTPDase) family (EC 3.6.1.5) comprise the dominant ectonucleotidases controlling the hydrolysis of nucleoside diphosphates and triphosphates (15, 52, 62). Some human and murine hepatoma cell lines express high levels of ENTPDase 2, which displays high ectoATPase activity and low ectoADPase activity. Under these conditions, ADP is thought to accumulate whereas adenosine production is delayed (37). Although adenosine has been shown to stimulate RVD of human erythrocytes (48), there are currently no reports, for any type of cell, of extracellular ADP affecting RVD.

In the present study we used Huh-7 hepatoma cells to determine whether ATP release, ATP_e hydrolysis, P receptor signaling, and RVD are functionally related. Our approach included an assessment of time-dependent volume changes of cells exposed to hypotonicity, the kinetics of ATP_e accumulation, and the extracellular hydrolysis of this nucleotide. Furthermore, RT-PCR was used to detect mRNAs of the main P receptor(s) and ENTPDase(s) involved in RVD control. Finally, we developed a simple data-driven mathematical model to account for the kinetics of ATP_e of swollen hepatoma cells.

Our results show that two mechanisms allow intracellular ATP to be released from Huh-7 hepatoma cells during hypotonic swelling and that ADP_e, derived from ATP_e hydrolysis, can activate $P2Y_{13}$ receptor to potentiate RVD.

MATERIALS AND METHODS

Chemicals

Cibacron blue 3GA, suramin, poly-L-lysine, apyrase (grade III), 2-(methylthio)adenosine 5′-diphosphate (2MetSADP), forskolin, luciferin, and luciferase were purchased from Sigma (St. Louis, MO). The acetoxymethyl (AM) esters of calcein and fura-2 were obtained from Molecular Probes (Eugene, OR). [γ^{32}P]ATP was from NEN Life Science Products (Boston, MA). Polyoxometalate-1 (POM-1) was from Tocris Bioscience. 2-[(2-Chloro-5-nitrophenyl)azo]-5-hydroxy-6-methyl-3-[(phosphonooxy)methyl]-4-pyridinecarboxaldehyde (MRS2211) was from Tocris Bioscience.

For Western blot analysis of P receptors, the anti-human $P2Y_{13}$ polyclonal antibody was purchased from Abcam (ab75103; Abcam, Cambridge, MA), and the anti-β tubulin antibody was from Sigma (St. Louis, MO). Immunoreactive bands were detected by chemiluminiscence (Amersham ECL plus Western Blotting Detection Reagents; GE Healthcare).

Purified Na^+-K^+-ATPase from pig kidney outer medulla was kindly provided by Dr. Monica Montes (IQUIFIB, School of Biochemistry and Pharmacy, University of Buenos Aires). It was prepared by the procedure of Jensen et al. (31). The enzyme had a specific activity of 8 U/mg. All other reagents were of analytical grade.

For RT-PCR analysis we used the following reagents: RNA isolation kit (Qiagen RNeasy, Hilden, Germany), reverse transcriptase M-MLV (Life Technologies, Berlin, Germany), Taq DNA polymerase (PB-L, Bio-Lógicos, Argentina-Brasil), and 1 μM of sense and antisense primers (Life Technologies, Berlin, Germany).

Cell Culture

Human hepatoma cells Huh-7 cells were cultured in DMEM supplemented with 10% vol/vol FBS and antibiotics (100 U/ml penicillin; 100 μg/ml streptomycin) in a humidified atmosphere of 5% CO_2 at 37°C. The viability was routinely assessed by retention of calcein and fura-2 using quantitative epifluorescence microscopy (20). No loss of cell viability was detected when Huh-7 cells were exposed to the different treatments used in this study.

Experimental Media

Cells were incubated during 45 min at 20°C in control isotonic medium (denoted as C) with the following composition (mM): 20 HEPES; 130 NaCl, 4.7 KCl, 1.5 $CaCl_2$, 1.2 KH_2PO_4, 1.2 $MgSO_4$, 5 $NaHCO_3$, 10 glucose, and 300 mosM osmolarity. (pH 7.4 at 20°C).

Hypotonic medium (denoted as H) was prepared by mixing one volume of medium C with one volume of medium D (medium C without NaCl), yielding an osmolarity of 180 mosM.

The osmolarity of all media was measured with a vapor pressure osmometer (5100 B; Wescor, Logan, UT).

Cell Volume

The technique was described in detail in previous reports (20, 49). Briefly, changes in cell water volume were inferred from readings of the fluorescence intensity recorded at 510 nm by exciting calcein at 495 nm. Hepatoma cells (5×10^4) were plated on 25-mm-diameter glass coverslips previously coated with poly-L-lysine. Each coverslip with attached cells was mounted on a perfusion chamber filled with medium C and placed on the stage of a Nikon TE-200 epifluorescence inverted microscope. Cells were loaded with 4 μM of calcein-AM for 1 h at room temperature.

Calcein-AM is nonfluorescent but, once loaded into cells, is cleaved by endogenous esterases to produce calcein, a highly fluorescent and well-retained dye.

Temporal changes in fluorescence intensity recorded from a small region of dye-loaded cells reflect changes in intracellular fluorophore concentration and, therefore, alterations of cell water volume (3, 4). Fluorescent images were acquired by using a charge coupled device camera (Hamamatsu C4742–95) connected to a computer and the Metafluor acquisition software (v. 5.0; Universal Imaging).

Experimental medium volume was 300 ul, except in experiments (see Fig. 5*C*), where "small volume" denotes an assay volume of 100 ul.

Values of Vr at different time points were computed from monitored changes in relative fluorescence (Ft/Fo), with Fo representing the signal obtained from a pinhole region of the cell equilibrated with isotonic medium, and Ft denoting the fluorescence of the same region of the cell at time *t*. Thus Vr represents a fractional volume, where volume before treatments is one, and volume changes are related to this value.

Data of Vr vs. time were used to estimate the extent of volume regulation or RVD, which was calculated as follows (see Ref. 3):

$$RVD = \frac{Vr_{max} - Vr_t}{Vr_{max} - 1} \times 100 \quad (1)$$

where Vr_{max} stands for the maximal value of Vr attained during hypotonic swelling, and Vr_t represents the value of Vr obtained at different times after reaching Vr_{max}. RVD thus represents the magnitude of volume regulation, with 100% RVD indicating complete volume regulation and 0% RVD indicating no volume regulation. We calculated the extent of RVD observed 40 min after Vr_{max}, so as to cover the whole time frame of the regulatory volume response studied. This parameter was denoted as RVD_{40}.

Preliminary experiments showed that exposure of cells to hypotonic medium at 20°C and 37°C provided similar values of RVD_{40}. Since online determinations of ATP_e had to be done at 20°C (see ATP_e determination below) to compare results of the different techniques, all experiments were made at that temperature.

Nucleotide Scavengers

Na^+-K^+-ATPase (5 U/ml) and apyrase (20 U/ml) dissolved in medium H were used as scavengers of extracellular nucleotides by accelerating the conversion from ATP to ADP + P_i (Na^+-K^+-ATPase) and from NTP to NMP + 2 P_i (apyrase), where NTP, NDP, and NMP stand for nucleoside tri-, di-, and monophosphate, respectively (50).

Agonists and Antagonists of P2 Receptors

The involvement of P2 receptors modulating RVD was characterized by using 1 μM 2MetSADP as a $P2Y_{13}$ agonist, 100 μM cibacron blue 3GA + 100 μM suramin (Cb + S) as P2Y antagonists, and 50 μM of MRS2211 as $P2Y_{13}$ antagonist.

EctoATPase Activity

Cell membranes are generally impermeable to low micromolar ATP concentrations added exogenously (57). Thus, when culture intact cells are used, any hydrolysis of extracellular ATP into ADP + P_i can be defined as ectoATPase activity and can be assigned to one or more membrane proteins of the ENTPDase superfamily (62). Thus we used an ATPase assay to determine the rate at which intact hepatoma cells hidrolyze the γ-terminal P_i of extracellular ATP (57).

Accordingly, ectoATPase activity (*vi*) was estimated by following the time course of [^{32}P]P_i release from [γ-^{32}P]ATP. Next, an exponential function was fitted to experimental data.

$$Y = Y_0 + A \times (1 - e^{-kt}) \quad (2)$$

where Y and Y_0 are the values of P_i at any time (t) and that at $t = 0$, A represents the maximal value for the increase of Y with time, and k is a rate coefficient. The parameters of best fit resulting from the regression were used to calculate the initial rate of ATP hydrolysis (*vi*) as $vi = k \times A$ (i.e., by taking the first derivative of *Eq. 2* for t tending to zero).

Exposure of cells to 100 μM POM-1 was used to inhibit ectoATPase activity.

Cytosolic Free Ca^{2+}

Changes in the concentration of cytosolic free calcium ($[Ca^{2+}]_i$) were determined by loading hepatoma cells with 6 μM of the Ca^{2+} sensitive fluorescent dye fura-2 AM. The procedure for fluorophore cell loading and extracellular washout, addition and removal of media, and acquisition of fluorescence intensity using a double-wavelength excitation system was described before (3). Briefly, 5×10^4 cells loaded with fura-2 were excited to alternate illumination at 340 and 380 nm and fluorescent emission images were recorded at 510 nm. The ratio 340/380 of the fluorescence intensities was calculated.

cAMP Assay

Two million cells were seeded in six-well plates in DMEM + FBS. After 24 h, the medium was removed and medium H supplemented with each treatment drug was added for 5 min. For cAMP extraction, medium was discarded and ethanol was added. The ethanol phase was dried and resuspended in 50 mM Tris·HCl, pH 7.4 and 0.1% BSA. cAMP was determined by competition of [^{3}H]cAMP for protein kinase A, as described previously (16). Forskolin (1 μM) was used to promote an increase in cAMP concentration.

RT-PCR Analysis

This technique was used to detect mRNAs of ENTPDases (subtypes 1–1, 1–2, 2, 3, and 8) and P2Y receptors (subtypes 12 and 13).

Total RNA was extracted from confluent cultures of Huh-7.

Synthesis of cDNA was performed using reverse transcriptase M-MLV (Life Technologies, Berlin, Germany) and random primers. PCR reactions were carried out in a 50-μl reaction volume containing the following reagents: 3 μl of cDNA preparation; 20 mM Tris·HCl, pH 8.0; 50 mM KCl; 1 mM $MgCl_2$; 0.25 mM of dATP, dGTP, dCTP, and dTTP; 5 U of Taq DNA polymerase, and 1 μM of sense and antisense primers. PCR was performed on a MasterCycler (Eppendorf, Hamburg, Germany), using the following conditions for denaturation, annealing, and extension (35 cycles): 95°C for 30 s, 55°C for 45 s, and 72°C for 1 min, followed by 72°C for 10 min. PCR products were separated by electrophoresis on a 2% agarose gel stained with ethidium bromide.

The specific primers sequences were as follows: *1*) for human ENTPDase 1–1 5′-gagagggagagagagatgaagag-3′and 5′-gttctgggtcaaccccacag-3′; *2*) for human ENTPDase 1–2, 5′-ctccagttttggtgctgtgaac-3′and 5′-gttctgggtcaaccccacag-3′; *3*) for human ENTPDase 2, 5′-tggaggcagc-cgcagtgaatgt-3′and 5′-ggaggcgaagagcagcaggaggac-3′; *4*) for human ENTPDase 3, 5′-accttcaactccagcacctg-3′and 5′-gtcaaaggcatgctcggagtg-3′; *5*) for human ENTPDase 8, 5′-cccccagaacctcacagttg-3′and 5′-acccagacgccgtagctctc-3′; *6*) for human $P2Y_{12}$, 5′-ccactctgcaggttgcaata-3′and 5′-taaatggcctggtggtcttc-3′; *7*) for human $P2Y_{13}$, 5′-ccagccctctaca-cagtggt-3′and 5′-gatcgtatttggcagggaga-3′; and *8*) for human plasma membrane Ca^{2+}-ATPase (PMCA), 5′-cctcccctgtggaaggtctgtctg-3′and 5′-tggttggtgttagagtcggtgtccctcgacctact-3′. The expected sizes of the PCR products were 485 bp for human ENTPDase 1-1, 200 bp for human ENTPDase 1-2, 314 bp for human ENTPDase 2-1, 245 bp for human ENTPDase 2-2, 402 bp for human ENTPDase 3, 504 bp for human ENTPDase 8-1, 393 bp for human ENTPDase 8-2, 475 bp for human $P2Y_{12}$, 399 bp for human $P2Y_{13}$, and 413 bp for human PMCA. PMCA was used as positive control.

Western Blot Analysis

Cells were incubated in cold lysis buffer (500 mM Tris·HCl pH 8, 150 mM NaCl, 1% Triton X-100, 5 mM EDTA, 0.1 mg/ml aprotinin, and 2 mM PMSF) 45 min, with vortexing every 5 min. Finally, samples were centrifuged at 12,000 *g* at 4°C for 10 min and supernatants were collected. $P2Y_{13}$ expression was determined in cell lysates; 20 ug of total protein were resolved by 10% SDS-PAGE. For immunoblotting, proteins were transferred to polyvinylidene fluoride membranes, which were then probed with an anti-human $P2Y_{13}$ polyclonal antibody (1:1,000) overnight at 4°C, followed by a 60-min incubation with horseradish peroxidase-conjugated secondary antibody. Protein loading in gels was evaluated by incubating membranes with an anti-β-tubulin antibody (1:1,000). Immunoreactive bands were detected by chemiluminiscence and quantified by densitometric analysis using ImageJ software (National Institutes of Health).

Measurement of ATP_e

The concentration of ATP_e was measured using firefly luciferase (EC 1.13.12.7), which catalyzes the oxidation of luciferin in the presence of ATP to produce light (11, 57).

Measurements were performed using 5×10^4 cells loaded on poly-L-lysine-coated coverslips which were mounted on a chamber of a custom-built luminometer, as described earlier (49). The setup allowed continuous measurements of ATP_e to be taken via the light output detection of the luciferin-luciferase reaction. Measurements were performed in 40 ul of experimental media (under the experimental conditions assay volume did not change with time), so that the medium has a height of ~104 μm (height at the coverslip bottom of the chamber equals 0). As shown by Okada et al. (46), measurements of ATP using this small volume provide similar results as the measurement of ATP at the cell surface using a surface-attached chimeric luciferase.

The time course of light emission was transformed into ATP_e concentration vs. time by means of a calibration curve by adding known exogenous ATP concentrations (0–200 nM). Calibration curves displayed a linear relationship within the range tested. Because luciferase activity at 37°C is only 10% of that observed at 20°C, to maintain full luciferase activity real-time ATP measurements were performed in a cool chamber acclimated at 20°C.

Measurement of ADP_e

The technique is based on the use of pyruvate kinase (PK) catalyzing the following reaction:

$$\text{ADP} + \text{phosphoenolpyruvate} \rightarrow \text{ATP} + \text{pyruvate}$$

The general idea is that all ADP present in the extracellular medium of a sample containing intact cells can be converted to ATP by PK; thus total ATP (ATP_T, the ATP present in the extracellular medium plus the ADP that was converted into ATP by PK) can be measured by the luciferin-luciferase reaction described above. By running separate measurements, in paired samples, of ATP_T and of ATP alone, the difference between these two provides an estimate of the ADP_e concentration.

Accordingly, 5×10^4 cells were seeded on coverslips using an experimental volume of 50 μl. At fixed time points, two 20-μl paired samples from the extracellular medium were taken. One of these samples was used for regular ATP measurements (*sample 1*), while the second sample was incubated 5 min at room temperature in the presence of PK (3 U) and 100 μM phosphoenolpyruvate to convert all ADP into ATP (ATP_T; *sample 2*). In both samples, the ATP concentration was measured by luminescence emission as described above. Values of ADP_e concentration were obtained by calculating ATP_T concentration from *sample 2* minus ATP concentration from *sample 1* (13).

Statistics

The effect of the different treatments on RVD was evaluated by means of one-way ANOVA followed by a Tukey-Kramer test of multiple comparisons. $P \leq 0.05$ was considered significant. For all experiments of Vr vs. time, 15–20 cells from 4–5 independent preparations were used.

RESULTS

Volume Regulation of Huh-7 Cells

Figure 1 shows time-dependent changes in Vr (volume relative to isotonic volume) for Huh-7 human hepatoma cells exposed to different experimental conditions. Under isotonic conditions (C) Vr remained constant, whereas exposure to a hypotonic medium (H) triggered a fast increase of Vr to a maximum (1.53 ± 0.04) followed by a slower volume decrease with RVD_{40} = 40.8 ± 7.80%. In similar experiments using a more prolonged hypotonic exposure (up to 130 min), cell volume achieved a steady state at Vr = 1.26 ± 0.03 after 60 min (data not shown).

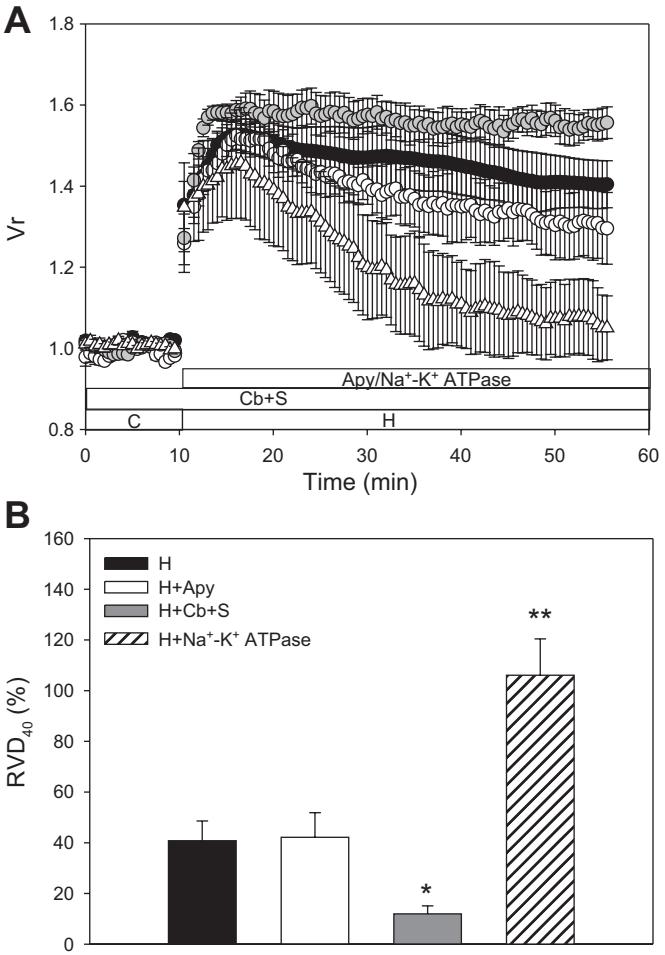

Fig. 1. Effects of P receptor antagonists and nucleotide scavengers on regulatory volume decrease. *A*: relative cell volume (Vr) as function of time in human hepatoma cells Huh-7 exposed to 300 mosM isotonic medium (C), followed by 180 mosM hypotonic medium (H) in the absence (black circles) or presence of apyrase (white circles) or Na^+-K^+-ATPase (white triangles). In separate experiments, cells preincubated 10 min in medium C with cibacron blue and suramin (Cb + S) were exposed to medium H with Cb + S (gray circles). *B*: RVD observed 40 min after the maximum Vr (RVD_{40}) estimated from experiments shown in *A*. Results are means ± SE of 50–60 cells from 4–5 independent experiments. *$P < 0.05$ vs. H; ** $P < 0.01$ vs. H.

In hypotonic medium plus apyrase (20 U/ml), on the other hand, the extent of volume regulation (RVD_{40} = 42.2 ± 9.71%) was not significantly different from that obtained in hypotonic medium alone, suggesting that extracellular di- and trinucleotides had no effect on RVD. Exposure of cells to hypotonic medium with 100 μM cibacron blue and 100 μM suramin (Cb + S, two well-known blockers of most P2 receptors) reduced RVD_{40} by 88% (RVD_{40} = 11.9 ± 3.17%).

On the other hand when exogenous Na^+-K^+-ATPase (5 U/ml), which promotes the extracellular conversion of ATP to ADP, was used combined with hypotonic medium, RVD_{40} amounted to 106.1 ± 14.3% ($P < 0.01$).

Up to here blockage of RVD by Cb + S would indicate that P2 receptors are important factors modulating the regulation of cell volume of hypotonically challenged Huh-7 cells. However, if this were true, then apyrase (which scavenges extracellular di- and trinucleotides) should inhibit RVD, but it did not. Moreover, Na^+-K^+-ATPase not only did not inhibit but en-

hanced RVD, indicating that ADP_e might be an important factor activating volume regulation. The experiments below were designed to clarify these issues.

Effects of Glibenclamide on RVD

The P2 blockers cibacron blue and suramin were reported to inhibit volume sensitive Cl^- channels (28, 29), so that the observed inhibition of RVD by both P2 blockers might be due to inhibition of Cl^- permeability. Accordingly, incubation of Huh-7 in hypotonic medium with the chloride channel blocker glibenclamide (400 μM) inhibited RVD to a similar extent than medium H + Cb + S (RVD_{40} = 17.5 ± 2.53 and 11.9 ± 3.17%, respectively; Fig. 2, *A* and *B*).

Glibenclamide has been shown to block cystic fibrosis transmembrane conductance regulator-dependent ATP efflux in various cell types (5). Thus, to discard that the observed effects of glibenclamide on Vr were due to blockage of ATP_e accumulation, cells were exposed to hypotonic medium with glibenclamide + 75 nM ATP. This ATP concentration is about twice the peak concentration of endogenous ATP_e obtained after hypotonic exposure of Huh-7 hepatoma cells. As shown in Fig. 2*B*, RVD_{40} in the presence of glibenclamide was similar in the absence or presence of exogenous ATP.

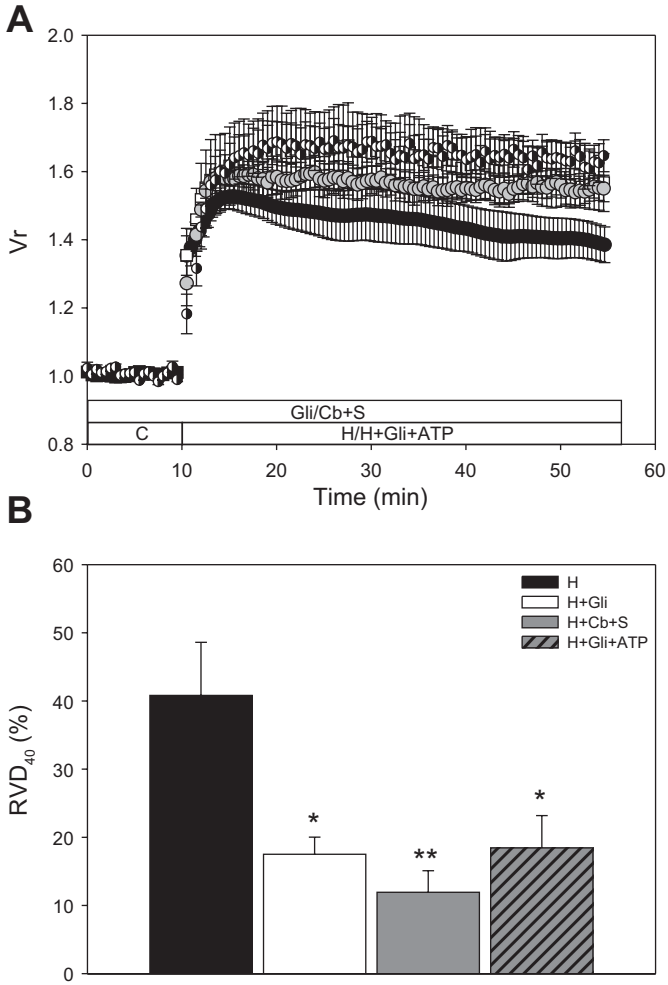

Fig. 2. Effects of inhibitors for Cl^- transport and P receptors on volume regulation. *A*: Vr as a function of time. Huh-7 cells were preincubated 10 min in isotonic medium C in the absence of inhibitors, or in the presence of glibenclamide (Gli; 400 μM) or cibacron blue (100 μM) and suramine (100 μM; Cb + S). At t = 10 min, cells were exposed to hypotonic medium (H) in the absence or presence of the same inhibitors, that is, H alone (black circles), H + Gli (white square), H + Cb + S (gray circles), or H + Gli + 75 nM ATP (half black, half white circles). *B*: values of RVD_{40} estimated from experiments shown in *A*. Results are means ± SE of 50–60 cells from 4–5 independent experiments. *$P < 0.05$ vs. medium H; **$P < 0.01$ vs. medium H. There were no statistical differences between H + Gli, H + Cb + S, and H + Gli + ATP.

Effects of Extracellular ADP on RVD

If, under hypotonic exposure of Huh-7 cells, exogenous Na^+-K^+-ATPase is enhancing RVD by facilitating ADP_e production from released ATP, then ADP_e or an ADP analog should also activate RVD. Accordingly, exposure of cells to medium H in the presence of 1 μM of the ADP agonist 2MetSADP induced a complete volume regulation (RVD_{40} = 107.9 ± 17.16%) that did not differ from that obtained in hypotonic medium containing Na^+-K^+-ATPase (Fig. 3, *A* and *B*).

After preincubating cells in isotonic medium with 5 μM MRS2211, a blocker of ADP receptor $P2Y_{13}$, followed by cells exposure to medium H + 2MetSADP + MRS2211, RVD_{40} amounted to 49.2 ± 5.94%, a value not significantly different to that obtained in the presence of medium H alone (Fig. 3, *A* and *B*).

Of the three known P receptors for ADP ($P2Y_1$, $P2Y_{12}$, and $P2Y_{13}$), $P2Y_1$ was reported to be nonfunctional in Huh-7 cells (56). Reverse transcriptase analysis showed the presence of mRNA for the $P2Y_{13}$ receptor but not for $P2Y_{12}$ (Fig. 3*C*), and Western blot analysis confirmed the presence of $P2Y_{13}$ in these cells (Fig. 3*D*).

Volume Regulation and Intracellular Signaling

Time-dependent changes in cytosolic free calcium (Ca_i^{2+}) were assessed continuously by fluorescence microscopy. For cells preincubated in isotonic medium, exposure to hypotonic medium in the absence or presence of 2MetSADP produced only a minor change in $[Ca^{2+}]_i$ concentration (Fig. 4, *A* and *B*), thus confirming that $P2Y_1$ receptor is not functional in these cells.

As shown in Fig. 3, we identified the $P2Y_{13}$ receptor in Huh-7 cells. The transduction mechanism of this ADP receptor subtype requires $G_{i/o}$ activation (1, 12), which might lead to inhibition of adenylyl cyclases, causing a decrease of cAMP concentration.

However, the concentration of cAMP in hypotonic medium did not change when 2MetSADP (activating $P2Y_{13}$) was present in cells exposed to hypotonic medium (Fig. 4*C*). Moreover, incubation of cells in hypotonic medium with forskolin (an activator of adenylyl cyclases) increased cAMP concentration sixfold, and this increase was not altered by 1 μM 2MetSADP.

Release of ATP and ADP_e Accumulation in Huh-7 Cells Under Hyposmolarity

Since exogenous Na^+-K^+-ATPase activity induced full RVD by promoting $ATP_e \rightarrow ADP_e$ conversion, we wondered whether the hypotonic challenge would be the mechanism enabling the release of ATP, with the resulting ATP_e being used as a substrate to generate ADP_e.

Incubation of Huh-7 cells in hypotonic medium triggered ATP release, so that ATP_e concentration increased acutely

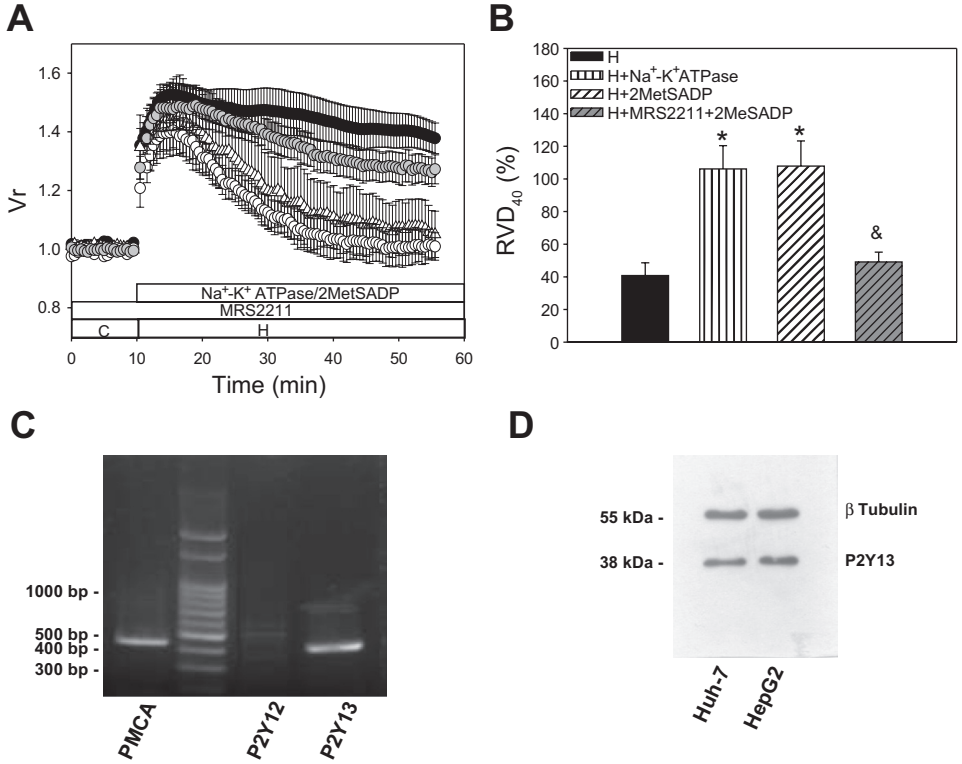

Fig. 3. Effect of ADP and P receptors on cell volume regulation. *A*: time course of Vr in isotonic and hypotonic media. Huh-7 cells were incubated in isotonic medium C, followed by hypotonic medium (H) in the absence (black circles) or presence of Na^+-K^+ ATPase (white triangles) or ADP agonist 2-(methylthio)adenosine 5′-diphosphate (2MetSADP; white circles). In separate experiments, cells preincubated 10 min in medium C + MRS 2211 (a $P2Y_{13}$ blocker) were exposed to medium H + 2MetSADP + MRS2211 (gray circles). *B*: values of RVD at 40 min after the maximum Vr estimated from experiments shown in *A*. Results are means ± SE of 50–60 cells from 4–5 independent experiments. *$P < 0.05$ vs. medium H; &$P < 0.05$ vs. either H + Na^+-K^+-ATPase or H + 2MetSADP. *C*: RT-PCR analysis of $P2Y_{12}$ and $P2Y_{13}$ receptors. Control amplifications were done using plasma membrane calcium ATPase (PMCA). *D*: Western blot analysis of $P2Y_{13}$ receptor in Huh-7 cells. *Lane 1* corresponds to Huh-7 cells, and *lane 2* corresponds to HepG2 cells, used as positive control. On the *left* markers of molecular mass (kDa) of each band are shown. On the *right*, band positions of the $P2Y_{13}$ receptor and β-tubulin are indicated. β-Tubulin was used to evaluate protein loading in the gel.

to a maximum [32.6 ± 10.87 nM × $(5 \times 10^4$ cells$)^{-1}$ at 15 min] followed by a slower decrease with $t_{1/2}$ = 16.2 ± 7.24 min.

Next, 10 μM carbenoxolone was used to block a conductive pathway of ATP release mediated by pannexin 1 (43), whereas brefeldin A was used to block ATP exocytosis. Both blockers produced a partial inhibition of ATP release with different kinetics (Fig. 5*A*).

Extracellular [ADP] increased from 1.2 ± 0.74 nM × $(5 \times 10^4$ cells$)^{-1}$ in isotonic conditions to 46.6 ± 16.07 nM × $(5 \times 10^4$ cells$)^{-1}$ at 15 min of the hypotonic treatment, leveling off thereafter [16.9 ± 4.14 nM × $(5 \times 10^4$ cells$)^{-1}$ at 60 min; Fig. 5*B*].

Volume Regulation Using a Small Assay Volume

If both ADP_e (produced by exogenous Na^+-K^+-ATPase) and 2MetSADP activate RVD (Figs. 1 and 3, *A* and *B*), and ADP_e is produced under hypotonicity (Fig. 5*B*), then a reduction of assay volume might enhance ADP_e concentration and activate RVD. Accordingly, a threefold reduction in assay volume (from 300 to 100 μl) produced an activation of RVD_{40} from 40.8 ± 7.80% (assay volume = 300 μl; Fig. 1) to 82.6 ± 4.31% (assay volume=100 μl, Fig. 5*C*; $P < 0.01$). This enhanced RVD_{40} was blocked in similar experiments using 50 μM MRS2211 (a blocker of $P2Y_{13}$) or 100 μM POM-1 (an inhibitor of ectoATPase activity), i.e., in a small hypotonic assay volume, RVD_{40} with MRS2211 (45.9 ± 3.93%) or POM-1 (25.8 ± 6.35%) did not differ from that obtained using a standard assay volume in the absence of these inhibitors.

Huh-7 Cells Showed ectoATPase Activity

For Huh-7 cells under hypotonicity, the observed decrease of $[ATP]_e$ after achieving a maximum suggests the existence of significant ectoATPase activity that can be assigned to one or more ectonucleotidases.

By following the release of $^{32}P_i$ from [^{32}γP]ATP we studied ectoATPase activity of intact Huh-7 cells under isotonic and hypotonic conditions in a wide range of, physiologically relevant, ATP concentrations (50–1,600 nM). EctoATPase activity was similar in hypo- and isotonic media (Fig. 6*A*) and increased with $[ATP]_e$ in an hyperbolic pattern, with $K_{0.5}$ = 333.2 ± 83.44 nM (Fig. 6*A*). In the lower part of the curve, the apparent rate constant describing ectoATPase activity was k_{ATP} = 0.15 ± 0.007 fmol P_i × (s × 5 × 10^4 cells$)^{-1}$ (Fig. 6*B*). This constant was used to model the kinetics of ATP_e accumulation as described in the APPENDIX.

Regarding the enzyme(s) responsible for ectoATPase activity, RT-PCR analysis of all ENTPDases subtypes allowed identification of a transcript only for ENTPDase 2 (Fig. 6*C*).

Modeling ATP_e Kinetics of Hypotonically Challenged Huh-7 Cells

The results above showed that swollen Huh-7 cells released ATP and that ectoATPase activity mediated ADP generation. We next built a mathematical model to quantify how these processes control ATP_e kinetics and to predict transmembrane ATP fluxes that mediate ATP release.

In the model, ATP release in hypotonically challenged Huh-7 cells is mediated by one or more nonlytic transport mechanisms collectively denoted as J_{NL}. Two J_{NL} subfluxes account for the fact that both brefeldin A (a blocker of exocytosis) and carbenoxolone (a blocker of conductive ATP release) were able to partially inhibit ATP_e accumulation.

Once in the extracellular medium, the model considers that ATP_e can be hydrolyzed by ectoATPase activity. Empirical

equations derived from experimental data of Fig. 5*A* and Fig. 6 were fed into the model (see APPENDIX for details). As shown in Fig. 7*A*, the model simulates the kinetics of ATP_e with reasonable accuracy, so that values of best fit for the different parameters could be obtained (see Table A1 of APPENDIX). Modeling shows the transition from a steady, isotonic $[ATP]_e$ level to nonlinear changes in ATP_e concentration under the different conditions (medium H, medium H + brefeldin A, and medium H + carbenoxolone).

The model predicts that the role of ectoATPase activity in determining ATP_e kinetics is important, since running the simulation, with best fit parameters, in the absence of ATP_e consumption (i.e., mathematically blocking the function describing ectoATPase activity vs. $[ATP]_e$) causes ATP_e concentrations to depart strongly from experimental data and attained much higher values (Fig. 7*A*, *inset*).

Figure 7*B* showed the predicted J_{NL} fluxes in the absence of inhibitors (J_{NL}) or in the presence of either brefeldin A (J_{NL}-H + BfA) or carbenoxolone (J_{NL}-H + Cbx). Following the hypotonic challenge, J_{NL} showed a steep, 12-fold increase to 7.8 ± 0.62 nM/min after 12 min, followed by a slower nonlinear decrease to a constant value of 4.4 ± 0.11 nM/min. Regarding the subfluxes, it can be seen that the nonexocytotic flux J_{NL}-H + BfA, representing conductive ATP release, was initially rapid, but unlike J_{NL} it decreased equally fast to a constant value of 1.9 ± 0.1 nM/min. The carbenoxolone insensitive flux, on the other hand, presented a different kinetics: there was a much slower initial increase (17-fold lower than J_{NL}-H + BfA) to a constant value where it remained constant thereafter (2.3 ± 0.10 nM/min). The sum of both partial fluxes was smaller than the total J_{NL} flux.

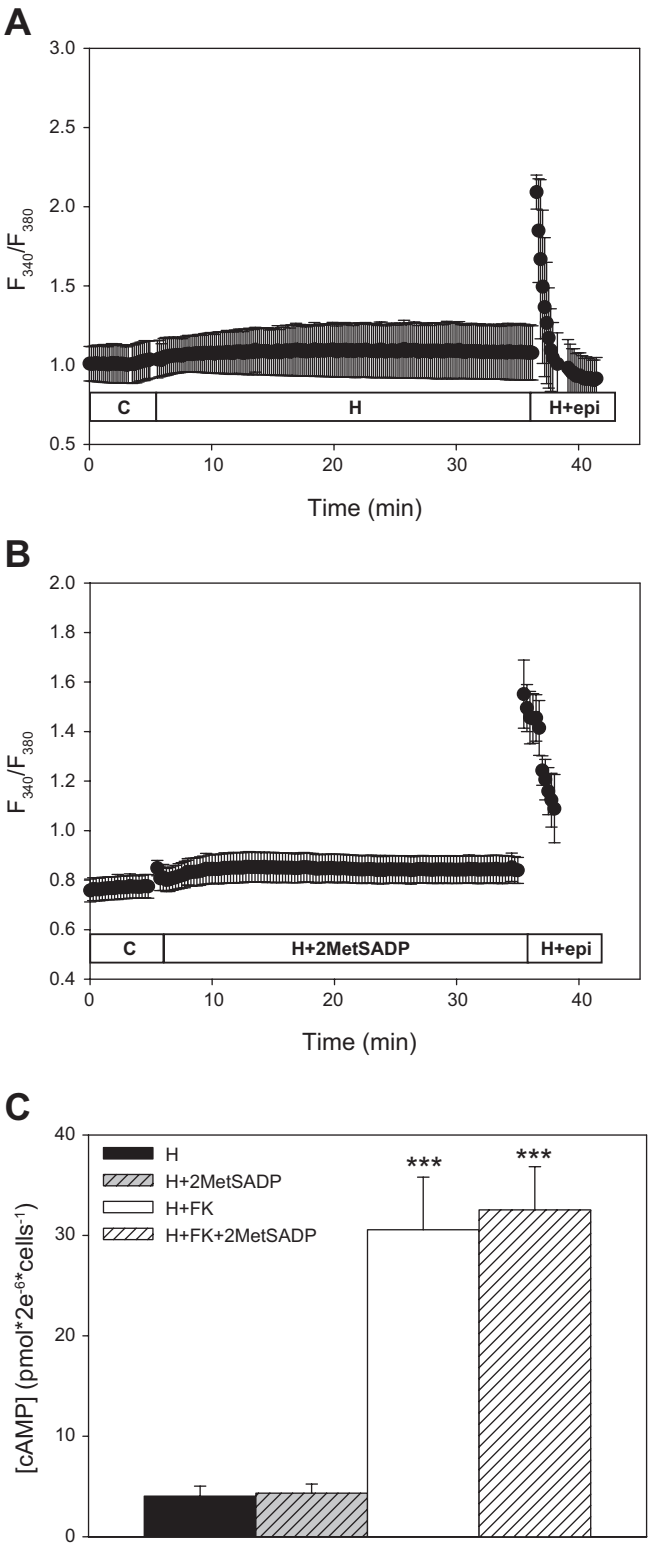

Fig. 4. Second messengers and cell volume regulation. *A*: effect of hypotonic medium on the concentration of cytosolic free calcium ($[Ca_i^{2+}]$). Cells incubated in isotonic medium (C), were exposed to hypotonic medium (H) and $[Ca^{2+}]_i$ was measured as the ratio of emission fluorescence intensities when excited at 340 and 380 nm (F_{340}/F_{380}). As a positive control epinephrine (epi; 10 μM) was added at the end of the experiments. Results are means ± SE of 50–60 cells from 4–5 independent experiments. *B*: $[Ca^{2+}]_i$ vs. time for cells exposed to medium C, followed by medium H + 2MetSADP (1 μM). At the end of the experiment epi (10 μM) was added. Results are means ± SE of 50–60 cells from 4–5 independent experiments. *C*: concentration of cAMP for cells exposed 5 min to hypotonic medium (H), medium H + 2MetSADP, medium H + forskolin (FK), or medium H + FK + 2MetSADP. Results are means ± SE of 8 independent experiments. ***$P < 0.0001$ vs. medium H or medium H + 2MetSADP.

DISCUSSION

Results show that Huh-7 cells, when exposed to hypotonicity, are able to release ATP and at the same time exhibit swelling followed by RVD.

A main goal of this study was to clarify how these processes are related, with special focus on the role of ATP release, ectoATPase activity and P receptor activation on volume regulation of Huh-7 cells.

Under hypotonicity, these cells exhibited an RVD_{40} amounting to 41%. At first glance, the fact that suramin + cibacron blue inhibited 71% of the RVD pointed to a role of P receptor signaling on volume regulation, but additional experiments contradicted this view. That is, addition of an excess of pure apyrase, a remover of extracellular di- and trinucleotides, did not affect RVD, while a similar treatment blunted the RVD response in different cell systems including hepatocytes from various vertebrate species and murine hepatoma cells (21, 50, 59).

The fact that in tracheal epithelium suramin and cibacron blue block Cl^- permeability (25), which is an effector of

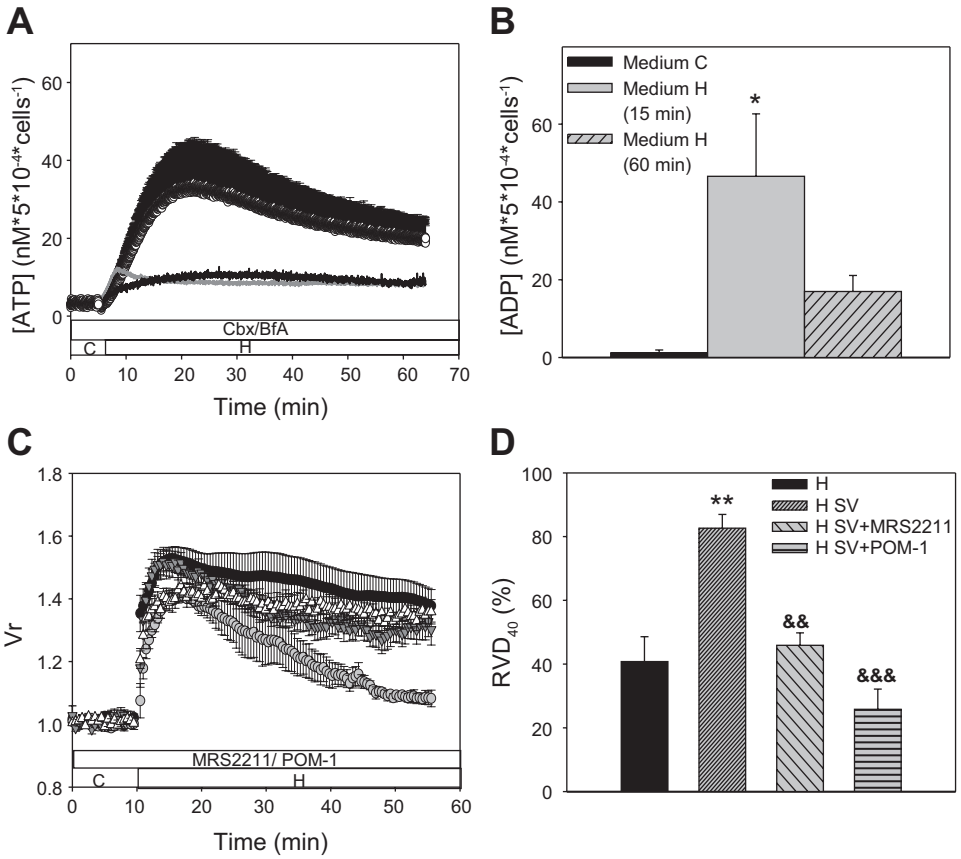

Fig. 5. Kinetics of extracellular (ATP_e) and cell volume, ADP_e concentration and RVD. *A*: time-dependent changes in ATP_e concentration for Huh-7 cells sequentially exposed to isotonic (C) and hypotonic (H) media. Cells were incubated in the absence of blockers (white circles) or in the presence of carbenoxolone (Cbx; 10 μM, black line) or brefeldin A (BfA; 2 ug/ml, gray line). Results are means ± SE from 4–5 independent experiments using 5×10^4 cells per experiment. To avoid data overlap, ATP_e determinations in the presence of Cbx and BfA are shown as mean values without their corresponding error bars. Results are means of 50–60 cells from 5 independent experiments. *B*: ADP_e concentration of cells incubated in isotonic medium (C) or in hypotonic medium (H) for 15 min or 60 min. Results are means of 4 independent experiments using 5×10^4 cells per experiment. Results are means ± SE of 50–60 cells from 4–5 independent experiments. $^*P < 0.05$ medium H (15 min) vs. medium C. *C*: Vr as function of time in human hepatoma cells Huh-7 exposed to 300 mosM isotonic medium (C), followed by 180 mosM hypotonic medium (H). Experiments were run in assay volume 300 μl (black circles) or 100 μl (gray circles). In small assay volume, cells were incubated in the absence of inhibitors (gray circles) or in the presence of 50 μM MRS2211 (inverted gray triangles) or 100 μM POM-1 (white triangles). Results are means ± SE of 50–60 cells from 4–5 independent experiments. *D*: calculated values of RVD_{40} taken from data of *C*. SV denotes small assay volume. $^{**}P < 0.01$ vs. medium H; $\&\&P < 0.01$ vs. H SV; $\&\&\&P < 0.001$ vs. H SV.

volume regulation in hepatic and hepatoma cells, would point to a direct effect of these compounds on the efflux of osmolytes during RVD. This is in line with experiments showing that glibenclamide, an inhibitor of volume-sensitive chloride channels (41), was able to block RVD of swollen Huh-7 hepatoma cells.

Thus, up to here, the lack of effect of apyrase should indicate that extracellular nucleotides were not mediating RVD. However, unexpectedly, addition of pure Na^+-K^+-ATPase to hypotonically exposed cells, far from removing RVD, it enhanced RVD_{40} from 41% to full volume regulation. Whereas apyrase activity is assumed to generate monophosphate nucleotides (AMP from ATP and/or UMP from UTP), which do not signal to P receptors, Na^+-K^+-ATPase promotes ATP_e hydrolysis to ADP_e. Thus there seems to be a basal RVD (i.e., $RVD_{40} \approx 40\%$) which, according to apyrase experiments, is independent of extracellular nucleotides, whereas in hypotonic medium containing an excess of exogenous Na^+-K^+-ATPase, all released ATP_e would be converted to ADP_e, with the latter being able to activate specific P receptors and further enhance RVD until cell volume is downregulated to near isotonic values (i.e., $RVD_{40} \approx 100\%$). To our knowledge there are no previous reports, for any cell type, of ADP_e, derived from ATP_e hydrolysis, strongly activating RVD.

In principle, three P2Y receptors are preferentially activated by ADP: $P2Y_1$, $P2Y_{12}$, and $P2Y_{13}$ (1). Activation of P2Y1 receptors is transduced as increases in $[Ca^{2+}]_i$, whereas $P2Y_{12}$ and $P2Y_{13}$ are linked to activation of G_i, which can lead to inhibition of adenylyl cyclases and therefore to a decrease of cAMP concentration. Despite the detection of $P2Y_1$ transcripts in both Huh-7 and HepG2 cells, almost no increase of $[Ca^{2+}]_i$ was observed in response to ADP_e, suggesting the lack of functional $P2Y_1$ receptors in these cell lines (30, 56). Similarly, in our hands, exposure of Huh-7 (and HepG2 cells; data not shown) to hypotonic medium, both in the absence and presence of 2MetSADP (a potent ADP-P2Y receptor agonist), did not affect Ca_i^{2+} (Fig. 4, *A* and *B*), thus suggesting the absence of

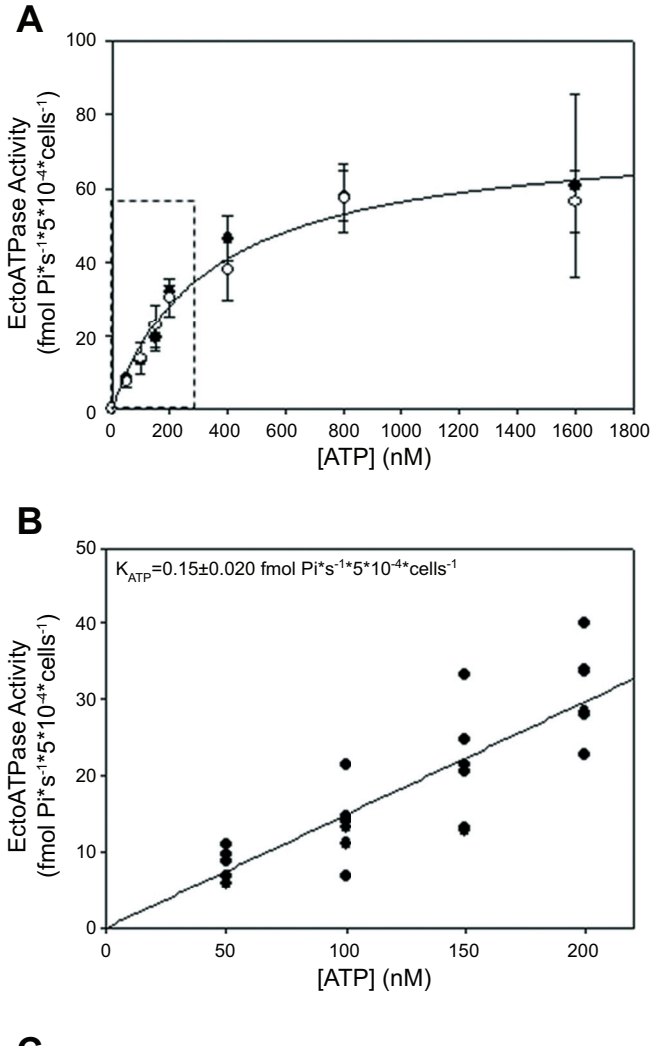

Fig. 6. EctoATPase activity vs. ATP_e concentration. *A*: cells were incubated with [γ-^{32}P]ATP in the presence of increasing concentrations of ATP (from 0 to 1,600 nM), both in medium C (black circles) and medium H (white circles). Each point represents the slope ± SE obtained by linear regression of a time course of [^{32}P]P_i release from [γ-^{32}P]ATP with at least five experimental points from 3 independent experiments. Continuous line shows the fit of a rectangular hyperbola to experimental data. *B*: similar to *A*, but only data from 0–200 nM are shown (black circles). *C*: RT-PCR analysis of mRNAs of ENTPDase subtypes (1–1, 1–2, 2, 3, 5, and 8) from Huh-7 cells. Control amplifications were done using PMCA.

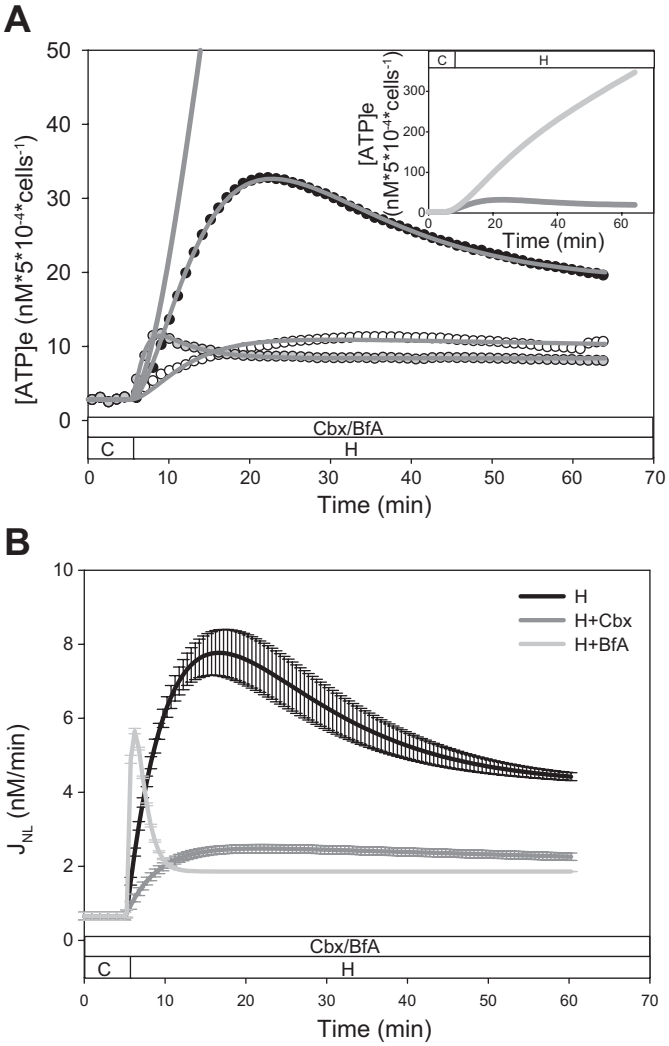

Fig. 7. Experimental and theoretical results of ATP_e kinetics in hypotonically challenged Huh-7 cells. *A*: experimental ATP_e kinetics of Fig. 5*A* (symbols) are shown together with the results of model dependent fit to experimental data (gray lines). Cells were incubated in medium H in the absence of inhibitors (black circles), or in the presence of carbenoxolone (H + Cbx, white circles) or brefeldin A (H + BfA, gray circles). Best fit values of the parameters and variables are given in Table A1 (see APPENDIX). *Inset*: model dependent simulation of $[ATP]_e$ kinetics in the absence (light gray lines) or presence (dark gray lines) of ectoATPase activity during the transition from isotonic medium to hypotonic medium. *B*: predicted J_{NL} fluxes in medium H in the absence of inhibitors (black lines), or in the presence of either Cbx (dark gray lines) or BfA (light gray lines).

a functional $P2Y_1$ receptor mediating ADP-induced Ca_i^{2+} mobilization.

On the other hand, our RT-PCR analysis revealed the presence of transcripts for $P2Y_{13}$, but not for $P2Y_{12}$ (Fig. 3*C*), and $P2Y_{13}$ was identified by Western blot analysis (Fig. 3*D*). As shown in Fig. 4*C*, for Huh-7 cells under hypotonicity, 2MetSADP alone or in combination with forskolin was unable to alter cAMP concentration.

Similarly, in Chinese hamster ovary cells expressing $P2Y_{13}$ receptor, exposure to nanomolar ADP_e did not modify cAMP levels (42).

As a last proof of the role of ADP-$P2Y_{13}$ on RVD, 2MetSADP led to a similar activation of RVD as that observed

in the presence of Na^+-K^+-ATPase, whereas the same ADP analog did not affect RVD when coincubated with MRS2211, a well-known blocker of $P2Y_{13}$ (34).

Despite the above described evidence for ADP_e involvement in autocrine/paracrine activation of RVD, a question remained open; if $ATP_e \rightarrow ADP_e$ conversion by exogenous Na^+-K^+-ATPase activity enhanced RVD, then endogenous ectoATPase activity (Fig. 6) should also increase ADP_e concentration to a certain extent and activate RVD. Then, apyrase hypotonic treatment, by removing ADP_e, should, at least partially, inhibit the RVD response, but this was not observed in our experiments (Fig. 1).

A possible explanation is that the lack of RVD activation by endogenous ADP_e, derived from the accumulated ATP_e, could be due to a relative low ectoATPase activity and the simultaneous dilution of ADP in the extracellular space. In this hypothetical scenario, reducing assay volume should lessen ADP_e diffusion, increasing ADP_e concentration at the surface of cells, thus activating RVD. Accordingly, when volumetric experiments of Fig. 1 were repeated in a 100-μl assay volume (a volume one-third of that used in all other volumetric experiments) an increase in RVD_{40} was observed. Moreover, this increase was blocked when similar experiments were run in the presence of the $P2Y_{13}$ blocker MRS2211 or in the presence of POM-1 (polyoxometalate-1), the latter a well-known blocker of ectoATPase activity (5). This means that either blocking $P2Y_{13}$ activation, or blocking the conversion of ATP_e to ADP_e by ectoATPase activity, both prevent ADP_e-mediated activation of RVD (Fig. 5*C*).

Among the eight subtypes of NTPDases that differ in tissue distribution and substrate preference, only ENTPDases 1, 2, 3, 5, and 8 are cell surface enzymes. Importantly, whereas ENTPDases 1, 3, and 8 display relative high ectoATPase and ectoADPase activities, only ENTPDase 2 exhibits a high ectoATPase-to-ectoADPase ratio (62). RT-PCR analysis on Huh-7 cells showed the presence of mRNA for ENTPDase 2 and the absence of mRNAs for all other ENTPDases (Fig. 6*C*). Thus the observed ectoATPase activity of these cells can be assigned to ENTPDase 2 (Fig. 6, *A* and *B*), whose activity should lead to the observed ADP_e accumulation.

The prevalence of ENTPDase 2 in Huh-7 has also been observed in other human hepatomas as HepG2 (60) and Li-7A, as well as in lung carcinoma (35). It has been suggested that its upregulated expression in these tumors might contribute to their proliferation by limiting apoptotic signaling by ATP_e. Thus the ability of tumor hepatomas to use ATP_e as a modulator of cell volume would be at risk, and ADP_e might have been selected to replace ATP_e as a signaling factor. Thus, although highly speculative to the moment, one could hypothesize a transition in the signaling process mediating RVD during the development of certain hepatic tumors. Human hepatocytes exhibit volume-dependent ATP release, with ATP_e-P2Y receptor interaction being a critical determinant of Cl^- permeability and cell volume regulation (21). The action of ATP_e is terminated by one or more ectonucleotidases like, e.g., ENTPDase 1. At least for human hepatoma Huh-7, the main activators of RVD are different, since following the hypotonic challenge, the exported ATP does not activate RVD but acts as a substrate for ENTPDase 2 to generate ADP_e, which can then interact with $P2Y_{13}$ receptors to enhance RVD.

Exposure of these cells to hypotonic medium led to a nonlinear increase in $[ATP_e]$ to a maximum, followed by a slower decay. In terms of the mathematical model proposed, the experimentally measured ATP_e kinetics is compatible with an acute increase of ATP efflux (J_{NL} in the model) to a maximum, followed by a slower decay towards a steady value significantly higher than the initial isotonic flux.

As shown in Fig. 7, intracellular ATP appears to be released by at least two independent mechanisms, since carbenoxolone, a well-known blocker of conductive ATP release, and brefeldin A, an inhibitor of exocytosis, were both able to partially decrease the time-dependent accumulation of ATP_e. Mathematical modeling showed that, upon hypotonic exposure, these two partial fluxes displayed different kinetics; the brefeldin A-resistant ATP flux increased acutely and decreased very rapidly to a final stationary value, while in the presence of carbenoxolone ATP efflux increased and decreased with much slower rates and did not reach a stationary value during the time interval of the experiments. The sum of both partial ATP fluxes was smaller than the total J_{NL} flux, pointing to the existence of an additional subflux insensitive to both carbenoxolone and brefeldin A.

Although exocytosis was implicated in hypotonically induced ATP release of HTC rat hepatoma, human hepatocytes and cholangiocytes (21, 23, 26), and turbot hepatocytes (47), no previous report of a carbenoxolone-sensitive component of ATP release was reported for either hepatic or hepatoma cells. Carbenoxolone at a 10-μM concentration has been used in many cell systems as a specific blocker of pannexin 1, which was postulated to form hexameric pores that allow passive transport of ATP across the plasma membrane (18).

The observed ATP_e kinetics does not only depend on the rate of ATP release but also on the capacity of ectonucleotidases to catalyze the hydrolysis of ATP_e. Indeed, Huh-7 cells exhibited a significant ectoATPase activity that displayed a linear dependence on ATP_e concentrations within a wide range of nanomolar concentrations (Fig. 6*B*). The model predicted that the role of ectoATPase activity in determining ATP_e kinetics is important, since running the simulation, with best fit parameters, in the absence of ATP_e degradation (i.e., mathematically blocking the function describing ectoATPase activity vs. $[ATP]_e$) caused ATP_e concentrations to depart strongly from experimental data and attained much higher values (Fig. 6*A*, *inset*).

Thus our observations support a model in which there are two distinct signaling pathways required for volume recovery after swelling of Huh-7 cells exposed to hypotonic medium. One pathway is independent of purinergic signaling and allows cells to recover their volume only partially (≈40%). The second pathway proposed involves full volume recovery from swelling through an ADP-$P2Y_{13}$ pathway. According to the scheme depicted in Fig. 8, hypotonic medium would trigger ATP release by exocytosis and one or more conductive pathways, with at least one of these mediated by pannexin 1. Once in the extracellular milieu, the ongoing conversion of ATP_e to ADP_e by ENTPDase 2 activity would promote the accumulated ADP to activate $P2Y_{13}$ receptors in a paracrine/autocrine manner, followed by a chain of intracellular events leading to efflux of ions and water, thus activating a regulatory response that provides full recovery of cell volume.

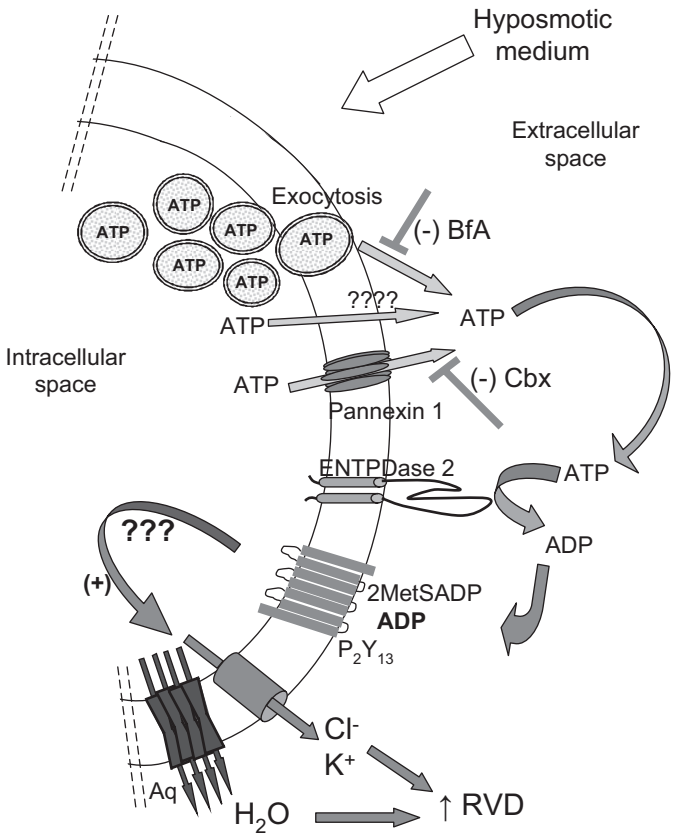

Fig. 8. Scheme depicting main mechanisms responsible for RVD of Huh-7 human hepatoma cells. Aq, aquaporin; +, activation; −, inhibition.

APPENDIX

Modeling of ATP_e Kinetics of Hypotonically Challenged Huh-7 Cells

A mathematical model was built to account for the experimentally observed ATP_e kinetics when Huh-7 cells were sequentially exposed to isotonic and hypotonic media.

In the model, $[ATP]_e$ is controlled by *1*) the rate of nonlytic ATP release (J_{NL}), which accounts for one or more mechanisms allowing ATP efflux in the absence of lysis, and *2*) the rate of ATP consumption by ectoATPase activity (J_V).

In the model, time-dependent changes in $[ATP]_e$ are given by

$$\frac{d[ATP]e}{dt} = J_{NL} - J_v \tag{3}$$

where J_{NL} and J_V are the fluxes of ATP release and of ATP hydrolysis, respectively.

Rate of ATP consumption (J_v). In the model, J_V denotes the flux of ATP consumption mediated by ectoATPase activity. The expression for J_V was derived empirically after analyzing data of ectoATPase activity assayed in intact Huh-7 cells under hypotonic conditions (i.e., similar conditions as those used to measure ATP_e kinetics) over an ample range of ATP_e concentrations (50–1,600 nM). In a first approach a hyperbolic function was fitted to experimental data of Fig. 6*A*.

$$J_v = \frac{V_{max}[ATP]_e}{K_{0.5} + [ATP]_e} \tag{4}$$

The term V_{max} represents the apparent maximal value of ectoATPase activity, and $K_{0.5}$ the concentration of ATP_e at which half-maximal activity is obtained, under the specific conditions of the experiment.

Since the model was used to simulate the experimentally obtained ATP_e concentrations, which lie at least eight times lower than the $K_{0.5}$, under this condition J_V can be best described by a linear function of $[ATP]_e$ as:

$$J_v = k_{ATP}[ATP_e] \tag{5}$$

$$\text{with } k_{ATP} = V_{max}/K_{0.5}. \tag{6}$$

Given that ectoATPase activity at different ATP concentrations is similar under isotonic and hypotonic conditions, it was assumed that k_{ATP} remained constant during the simulation.

Nonlytic release of ATP (J_{NL}). Following hypotonic exposure of Huh-7 cells, the nonlinear accumulation of ATP_e observed in Fig. 5*A* can be explained by assuming time-dependent changes in the flux of ATP release (J_{NL}), which can be modeled as the transition through three different states of flux. Accordingly, in the unstimulated condition, there is a basal, isotonic, stationary state of flux (*i*). The hypotonic stimulus induces a transition to a stimulated state (*s*), followed by a final stationary state (*f*). The isotonic-hypotonic transition is formulated as the following irreversible two-step process:

$$x_i \rightarrow x_s \rightarrow x_f \tag{7}$$

as mentioned above x_i, x_s, and x_f represent fractional contributions to total ATP release (see Fig. A1).

These quantities display values from 0 to 1 and at every time are related by:

$$x_i + x_s + x_f = 1 \tag{8}$$

The net flux of ATP release is given by:

$$J_{NL} = x_i \cdot J_i + x_s \cdot J_s + x_f \cdot J_f \tag{9}$$

As such J_{NL} is fully determined by the sum of each of three states (*i*, *s*, and *f*). Since J_i, J_s, and J_f do not change with time, the time course of J_{NL} is controlled by the time dependence of x_i, x_s, and x_f.

Before the hypotonic stimulus,

$$x_i^0 = 1$$
$$x_s^0 = x_f^0 = 0$$
$$J_{NL}^0 = J_i$$

To simulate the transition from isotonic to hypotonic conditions, these values are held constant until the stimulus is applied.

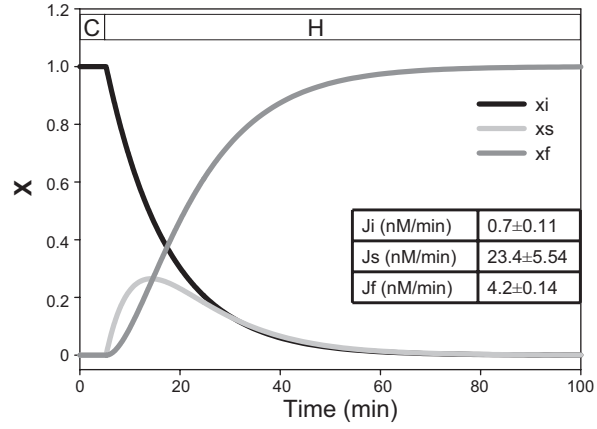

Fig. A1. Parameters used for modeling ATP fluxes. As explained in APPENDIX, time-dependent changes in J_{NL} are calculated as

$$J_{NL} = x_i \cdot J_i + x_s \cdot J_s + x_f \cdot J_f$$

with each "*x*" subtype (x_i, x_s, and x_f) representing a fractional contribution to total ATP release. *Inset*: best fitting values of J_i, J_s, and J_f in the absence of inhibitors (see Fig. 7*B* and Table A1).

The final state is given by:

$$x_i^\infty = x_s^\infty = 0 \qquad x_f^\infty = 1$$
$$J_{NL}^\infty = J_f$$

Upon hypotonic exposure, the kinetics of the activation process given in *Eq. 7* is governed by the following differential equations:

$$\frac{dx_i}{dt} = -k_1 x_i \tag{10}$$

$$\frac{dx_s}{dt} = k_1 x_i - k_2 x_s \tag{11}$$

$$\frac{dx_f}{dt} = k_2 x_s \tag{12}$$

where k_1 and k_2 are first order rate constants for the first and second transition, respectively.

Given the boundary conditions, and assuming $k_1 \neq k_2$, the set of differential *Eqs. 10–12* can be analytically solved to obtain the time dependence of x_i, x_s, and x_f:

$$x_i = e^{-k_1(t-t_{st})} \tag{13}$$

$$x_s = \frac{k_1}{k_1 - k_2}\left[e^{-k_2(t-t_{st})} - e^{-k_1(t-t_{st})}\right] \tag{14}$$

$$x_f = 1 - x_i - x_s = \frac{k_1\left[1 - e^{-k_2(t-t_{st})}\right] - k_2\left[1 - e^{-k_1(t-t_{st})}\right]}{k_1 - k_2} \tag{15}$$

where t_{st} represents the time at which the hypotonic stimulus is applied (see Fig. A1).

Introducing these expressions into *Eq. 9* we obtain the following biexponential function for the time dependence of J_{NL}:

$$J_{NL} = J_i + A_1^J\left[1 - e^{-k_1(t-t_{st})}\right] + A_2^J\left[1 - e^{-k_2(t-t_{st})}\right] \tag{16}$$

$$A_1^J = \frac{k_1 J_e - k_2 J_f}{k_1 - k_2} - \mathrm{J_i} \tag{17}$$

$$A_2^J = \frac{k_1}{k_1 - k_2}(J_s - J_f) \tag{18}$$

This equation allows J_{NL} to increase from a initial value (i.e., J_i) to a final value (i.e., J_f) either monotonously or going through a maximum as in J_{NL}-BfA and J_{NL}-Cbx (Fig. 7*B*).

Time course of ATP$_e$ accumulation. Having defined expressions for both J_V and J_{NL}, we can now integrate the differential equation that rules the kinetics of ATP_e concentration (*Eq. 3*) to obtain, in the general case of $k_1 \neq k_2$, the following triexponential function of time:

$$\int_0^t \frac{d[\mathrm{ATP_e}]}{dt}dt = [\mathrm{ATP_e}] - [\mathrm{ATP_e}]^0 = A_{\mathrm{ATP}}^A\left[1 - e^{-k_{\mathrm{ATP}}(t-t_{st})}\right] + A_1^A\left[1 - e^{-k_1(t-t_{st})}\right] + A_2^A\left[1 - e^{-k_2(t-t_{st})}\right] \tag{19}$$

where the amplitudes of the exponential terms are given by:

$$A_1^A = -\frac{J_i}{k_{\mathrm{ATP}} - k_1} + \frac{k_1 J_s - k_2 J_f}{(k_{\mathrm{ATP}} - k_1)\cdot(k_1 - k_2)} = \frac{A_1^J}{(k_{\mathrm{ATP}} - k_1)} \tag{20}$$

$$A_2^A = -\frac{(J_s - J_f)k_1}{(k_{\mathrm{ATP}} - k_2)\cdot(k_1 - k_2)} = \frac{A_2^J}{(k_{\mathrm{ATP}} - k_2)} \tag{21}$$

$$A_{\mathrm{ATP}}^A = -\frac{J_f - J_i}{k_{\mathrm{ATP}}} + \frac{J_i}{k_{\mathrm{ATP}} - k_1} - \frac{k_1 J_s - k_2 J_f}{(k_{\mathrm{ATP}} - k_1)\cdot(k_1 - k_2)} + \frac{(J_s - J_f)k_1}{(k_{\mathrm{ATP}} - k_2)\cdot(k_1 - k_2)} = \frac{J_f - J_i}{k_{\mathrm{ATP}}} - A_1^A - A_2^A \tag{22}$$

Thus the model involves six parameters in all: J_i, J_s, J_f, k_{ATP}, k_1, and k_2. As mentioned above, k_{ATP} was derived from the experimental measure of ATPase activity at different ATP_e concentrations. In addition, given that the isotonic ATP_e concentration remains steady, we assumed $J_i = J_V$ at that particular ATP_e concentration, so that:

$$J_i = k_{\mathrm{ATP}} \cdot [\mathrm{ATP}]_e \tag{23}$$

In this way, there are four parameters left to be estimated by fitting the model to the experimental results, i.e, J_s, J_f, k_1, and k_2.

Similarly, as time increases the ATP_e concentration approaches a final stationary value given by:

$$[\mathrm{ATP_e}]^\infty = \frac{J_f}{k_{\mathrm{ATP}}} \tag{24}$$

Equation 19 in the model shows that $[ATP]_e$ is a triexponential function of time, with three different amplitudes allowing an initial rise to a maximal value of $[ATP]_e$, followed by a decay to a constant value that may be different from the initial, isotonic value (i.e., if $J_i \neq J_f$).

The same model describing $[ATP]_e$ kinetics was fitted to experimental data when cells were exposed to hypotonic medium in the presence of either brefeldin A or carbenoxolone, with results shown in Fig. 7*A*.

Table A1 shows the fixed and best fit values of the model parameters.

Preliminary tests. When building the model, we tried alternative, more simple models which did not provide an accurate fit to experimental data of Fig. 7*A*, since:

Table A1. *Parameters of the model*

Flux/Parameter/Medium	Value	Unit
J_v		
$>k_{ATP}$		
H (c)	0.2 ± 0.03	min^{-1}
J_{NL}		
J_i		
I (c)	0.7 ± 0.11	nM/min
J_s		
H (bf)	23.4 ± 5.54	nM/min
H + Cbx (bf)	177.8 ± 12.44	nM/min
H + BfA (bf)	13.3 ± 0.18	nM/min
J_f		
H (bf)	4.2 ± 0.14	nM/min
H + Cbx (bf/c)	0 ± 0	nM/min
H + BfA (bf)	1.86 ± 0.004	nM/min
k_1		
H (bf)	0.08 ± 0.018	min^{-1}
H + Cbx (bf)	0.003 ± 0.0002	min^{-1}
H + BfA (bf)	1.14 ± 0.0203	min^{-1}
k_2		
H (bf)	0.15 ± 0.025	min^{-1}
H + Cbx (bf)	0.25 ± 0.006	min^{-1}
H + BfA (bf)	1.14 ± 0.020	min^{-1}

Results are values of best fit obtained by fitting the model to experimental data. c, Constant value; bf, best fitting value; J_{NL}, nonlytic flux of ATP release; J_v, rate of ATP consumption by ecto-ATPase activity, with k_{ATP} being the apparent first order constant; k_{ATP}, calculated by fitting an exponential function to data of Fig. 6*A* and using *Eqs. 5–7* of APPENDIX; J_i, flux of ATP release in isotonic medium (computed from values of k_{ATP} and extracellular ATP concentration in isotonic conditions according *to Eq. 23*); J_s and J_f, activated flux of ATP and final stationary flux of ATP under hypotonic conditions, respectively (J_f was considered a fitting parameter (bf), except when cells were incubated in the presence of carbenoxolone, where J_f was considered 0); H, hypotonic medium; H + Cbx, hypotonic medium + carbenoxolone; H + BfA, hypotonic medium + brefeldin A. When cells were exposed to H + BfA, k_2 was assumed equal to k_1 (see APPENDIX).

1) A two-state model, in which there is a single transition from the initial to the final state ($x_i \rightarrow x_f$), predicts a monotonous increase of $[ATP]_e$, no matter whether this transformation is reversible or irreversible, and thus could not explain the experimentally observed ATP_e kinetics.

2) By assuming a three state model (x_i, x_s, and x_f), similar to the final model used for the simulations (i.e., *Eq. 9*), except that $J_i = J_f$ (i.e., an homeostatic response of the flux), the simulation fitted to experimental data, but according to the Akaike criterion (2), the bias was much larger than in the model presented in this study, where Ji≠Jf.

Model fitting. Best fitting values for J_s, J_f, k_1, and k_2 and their associated standard errors were obtained with Copasi software, version 4.7. The Copasi file describing the model is available upon request.

Simulations were run in Libreoffice 3.3. 4 spreadsheets by introducing the integrated equations for $[ATP]_e$ and J_{NL}. Standard errors for mean J_{NL} values (Fig. 7) were computed from the covariance matrix of the model parameters using the approximated formula:

$$\mathrm{Var}(Z) = \sum \left(\frac{\partial Z}{\partial Y_i}\right)^2 \cdot \mathrm{Var}(X_i) - 2 \cdot \sum \left(\frac{\partial Z}{\partial Y_i}\right) \cdot \left(\frac{\partial Z}{\partial Y_j}\right) \cdot \mathrm{Cov}(Y_i, Y_j)$$

where Z is a random variable that is a function of random variables Y_i.

ACKNOWLEDGMENTS

We thank Dr. M. F. Troncoso and Dr. M. C. Larocca for helpful discussion of this study and D. Malena Manzi and Alejandro Carozzo for technical advice.

GRANTS

This work was supported by Grants PICT 0151 (to P. J. Schwarzbaum) and PICT 07-0712 (to M. V. Espelt) from Agencia Nacional de Promoción Científica y Tecnológica, Grant PIP 112 20110100639 from Consejo Nacional de Investigaciones Científicas y Técnicas (CONICET), and UBACYT 20020100100090 from University of Buenos Aires.

DISCLOSURES

No conflicts of interest, financial or otherwise, are declared by the author(s).

AUTHOR CONTRIBUTIONS

Author contributions: M.V.E. and P.J.S. conception and design of research; M.V.E., F.d.T.P., C.L.A., G.S.A., J.I., M.F.L.D., and C.D. performed experiments; M.V.E., C.L.A., J.I., and C.D. analyzed data; M.V.E., C.D., and P.J.S. interpreted results of experiments; M.V.E. prepared figures; M.V.E. and P.J.S. drafted manuscript; M.V.E. and P.J.S. edited and revised manuscript; M.V.E. and P.J.S. approved final version of manuscript.

REFERENCES

1. **Abbracchio MP, Burnstock G, Boeynaems JM, Barnard EA, Boyer JL, Kennedy C, Knight GE, Fumagalli M, Gachet C, Jacobson KA, Weisman GA.** Update on the P2Y G protein-coupled nucleotide receptors: from molecular mechanisms and pathophysiology to therapy. *Pharmacol Rev* 58: 281–341, 2006.
2. **Akaike H.** Data analysis by statistical models. *No To Hattatsu* 24: 127–133, 1992.
3. **Altamirano J, Brodwick MS, Alvarez-Leefmans FJ.** Regulatory volume decrease and intracellular Ca^{2+} in murine neuroblastoma cells studied with fluorescent probes. *J Gen Physiol* 112: 145–160, 1998.
4. **Alvarez-Leefmans FJ, Altamirano J, Crowe WE.** Use of ion-selective microelectrodes and fluorescent probes to measure cell volume. *Meth Neurosci* 27: 361–391, 1995.
5. **Becq F.** CFTR channels and adenosine triphosphate release: the impossible rendez-vous revisited in skeletal muscle. *J Physiol* 588: 4605–4606, 2010.
6. **Blum AE, Walsh CB, Dubyak GR.** Extracellular osmolarity modulates G protein-coupled receptor-dependent ATP release from 1321N1 astrocytoma cells. *Am J Physiol Cell Physiol* 298: C386–C396, 2010.
7. **Bodin P, Bailey D, Burnstock G.** Increased flow-induced ATP release from isolated vascular endothelial but not smooth muscle cells. *Br J Pharmacol* 103: 1203–1205, 1991.
8. **Bourdreault F, Grygorczyk R.** Cell swelling-induced ATP release is tightly dependent on intracellular calcium elevations. *J Physiol* 561: 499–513, 2004.
9. **Braunstein GM, Roman RM, Clancy JP, Kudlow BA, Taylor AL, Shylonsky VG, Jovov B, Peter K, Jilling T, Ismailov II, Benos DJ, Schwiebert LM, Fitz JG, Schwiebert EM.** Cystic fibrosis transmembrane conductance regulator facilitates ATP release by stimulating a separate ATP release channel for autocrine control of cell volume regulation. *J Biol Chem* 276: 6621–6630, 2001.
10. **Braunstein GM, Zsembery A, Tucker TA, Schwiebert EM.** Purinergic signaling underlies CFTR control of human airway epithelial cell volume. *J Cyst Fibros* 3: 99–117, 2004.
11. **Brown AM.** ATP and ATPase determinations in red blood cells. In: *Red Cell Membranes, A Methodological Approach*, edited by Ellory JC, Young JD. New York: Academic, 1980.
12. **Burnstock G.** Purine and pyrimidine receptors. *Cell Mol Life Sci* 64: 471–483, 2007.
13. **Burrell HE, Wlodarski B, Foster BJ, Buckley KA, Sharpe GR, Quayle JM, Simpson AW, Gallagher JA.** Human keratinocytes release ATP and utilize three mechanisms for nucleotide interconversion at the cell surface. *J Biol Chem* 280: 29667–29676, 2005.
14. **Chara O, Espelt MV, Krumschnabel G, Schwarzbaum PJ.** Regulatory volume decrease and P receptor signaling in fish cells: mechanisms, physiology, and modeling approaches. *J Exp Zool A Ecol Genet Physiol* 315: 175–202, 2011.
15. **Corriden R, Insel PA.** Basal release of ATP: an autocrine- paracrine mechanism for cell regulation. *Sci Signal* 3: re1, 2010.
16. **Davio CA, Cricco GP, Bergoc RM, Rivera ES.** H1 and H2 histamine receptors in experimental carcinomas with an atypical coupling to signal transducers. *Biochem Pharmacol* 50: 91–96, 1995.
17. **Dezaki K, Tsumura T, Maeno E, Okada Y.** Receptor-mediated facilitation of cell volume regulation by swelling-induced ATP release in human epithelial cells. *Jpn J Physiol* 50: 235–241, 2000.
18. **Dubyak GR.** Both sides now: multiple interactions of ATP with pannexin-1 hemichannels. Focus on "A permeant regulating its permeation pore: inhibition of pannexin 1 channels by ATP". *Am J Physiol Cell Physiol* 296: C235–C241, 2009.
19. **Dutta AK, Sabirov RZ, Uramoto H, Okada Y.** Role of ATP-conductive anion channel in ATP release from neonatal rat cardiomyocytes in ischaemic or hypoxic conditions. *J Physiol* 559: 799–812, 2004.
20. **Espelt MV, Mut PN, Amodeo G, Krumschnabel G, Schwarzbaum PJ.** Volumetric and ionic responses of goldfish hepatocytes to anisotonic exposure and energetic limitation. *J Exp Biol* 206: 513–22, 2003.
21. **Feranchak AP, Fitz JG, Roman RM.** Volume-sensitive purinergic signaling in human hepatocytes. *J Hepatol* 33: 174–182, 2000.
22. **Feranchak AP, Lewis MA, Kresge C, Sathe M, Bugde A, Luby-Phelps K, Antich PP, Fitz JG.** Initiation of purinergic signaling by exocytosis of ATP-containing vesicles in liver epithelium. *J Biol Chem* 285: 8138–8147, 2010.
23. **Fitz JG.** Regulation of cellular ATP release. *Trans Am Clin Climatol Assoc* 118: 199–208, 2007.
24. **Friedrich B, Matskevich I, Lang F.** Cell volume regulatory mechanisms. *Contrib Nephrol* 152: 1–8, 2006.
25. **Galietta LJ, Falzoni S, Di Virgil F, Romeo G, Zegarra-Moran O.** Characterization of volume-sensitive taurine- and Cl^--permeable channels. *Am J Physiol Cell Physiol* 273: C57–C66, 1997.
26. **Gatof D, Kilic G, Fitz JG.** Vesicular exocytosis contributes to volume-sensitive ATP release in biliary cells. *Am J Physiol Gastrointest Liver Physiol* 286: G538–G546, 2004.
27. **Haussinger D, Kubitz R, Reinehr R, Bode JG, Schliess F.** Molecular aspects of medicine: from experimental to clinical hepatology. *Mol Aspects Med* 5: 221–360, 2004.
28. **Hazama A, Fan HT, Abdullaey I, Maeno E, Ando-Akatsuka Y, Okada Y.** Swelling-activated, cistic fibrosis transmembrane conductance regulator-augmented ATP release and Cl^- conductances in murine C127 cells. *J Physiol* 523: 1–11, 2000.
29. **Hoffmann EK, Pedersen SF.** Cell volume homeostatic mechanisms: effectors and signalling pathways. *Acta Physiol (Oxf)* 202: 465–485, 2011.
30. **Jacquet S, Malaval C, Martinez LO, Sak K, Rolland C, Perez C, Nauze M, Champagne E, Tercé F, Gachet C, Perret B, Collet X, Boeynaems JM, Barbaras R.** The nucleotide receptor P2Y13 is a key

regulator of hepatic high-density lipoprotein (HDL) endocytosis. *Cell Mol Life Sci* 62: 2508–2515, 2005.
31. **Jensen J, Nørby JG, Ottolenghi P.** Binding of sodium and potassium to the sodium pump of pig kidney evaluated from nucleotide binding behaviour. *J Physiol* 346: 219–241, 1984.
32. **Junankar PR, Karjalainen A, Kirk K.** The role of P2Y1 purinergic receptors and cytosolic Ca^{2+} in hypotonically activated osmolyte efflux from a rat hepatoma cell line. *J Biol Chem* 277: 40324–40334, 2002.
33. **Kim HD, Bowen JW, James-Kracke MR, Landon LA, Camden JM, Burnett JE, Turner JT.** Potentiation of regulatory volume decrease by P2U purinoceptors in HSG-PA cells. *Am J Physiol Cell Physiol* 270: C86–C97, 1996.
34. **Kim YC, Lee JS, Sak K, Marteau F, Mamedova L, Boeynaems JM, Jacobson JA.** Synthesis of pyridoxal phosphate derivatives with antagonist activity at the P2Y13 receptor. *Biochem Pharmacol* 70: 266–274, 2005.
35. **Knowles AF, Chiang WC.** Enzymatic and transcriptional regulation of human ecto-ATPase/E-NTPDase 2. *Arch Biochem Biophys* 418: 217–227, 2003.
36. **Koyama T, Oike M, Ito Y.** Involvement of Rho-kinase and tyrosine kinase in hypotonic stress-induced ATP release in bovine aortic endothelial cells. *J Physiol* 532: 759–769, 2001.
37. **Kukulski F, Lévesque SA, Lavoie EG, Lecka J, Bigonnesse F, Knowles AF, Robson SC, Kirley TL, Sévigny J.** Comparative hydrolysis of P2 receptor agonists by NTPDases 1, 2, 3 and 8. *Purinergic Signal* 1: 193–204, 2005.
38. **Lang F.** Mechanisms and significance of cell volume regulation. *J Am Coll Nutr* 26: 613–623, 2007.
39. **Lazarowski ER, Boucher RC, Harden TK.** Mechanisms of release of nucleotides and integration of their action as P2X- and P2Y-receptor activating molecules. *Mol Pharmacol* 64: 785–795, 2003.
40. **Lazarowski ER.** Vesicular and conductive mechanisms of nucleotide release. *Purinergic Signal* 8: 359–73, 2012.
41. **Liu Y, Oiki S, Tsumura T, Shimizu T, Okada Y.** Glibenclamide blocks volume-sensitive Cl^- channels by dual mechanisms. *Am J Physiol Cell Physiol* 275: C343–C351, 1998.
42. **Marteau F, Le Poul E, Communi D, Communi D, Labouret C, Savi P, Boeynaems JM, Suarez Gonzalez N.** Pharmacological characterization of the human P2Y13 receptor. *Mol Pharmacol* 64: 104–112, 2003.
43. **Montalbetti N, Leal Denis MF, Pignataro OP, Kobatake E, Lazarowski ER, Schwarzbaum PJ.** Homeostasis of extracellular ATP in human erythrocytes. *J Biol Chem* 286: 38397–38407, 2011.
44. **Nandigama R, Padmasekar M, Wartenberg M, Sauer H.** Feed forward cycle of hypotonic stress-induced ATP release, purinergic receptor activation, and growth stimulation of prostate cancer cells. *J Biol Chem* 281: 5686–5693, 2006.
45. **Oike M, Kimura C, Koyama T, Yoshikawa M, Ito Y.** Hypotonic stress-induced dual Ca^{2+} responses in bovine aortic endothelial cells. *Am J Physiol Heart Circ Physiol* 279: H630–H638, 2000.
46. **Okada SF, Nicholas RA, Kreda SM, Lazarowski ER, Boucher RC.** Physiological regulation of ATP release at the apical surface of human airway epithelia. *J Biol Chem* 281: 22992–23002, 2006.
47. **Ollivier E, Pichavant-Rafini K, Puill-Stephan E, Calves P, Nonnotte L, Nonnotte G.** Effects of hypo-otonic stress on ATP release in isolated turbot (Scophthalmus maximus) hepatocytes. *Biol Cell* 98: 427–437, 2006.
48. **Pafundo DE, Alvarez CL, Krumschnabel G, Schwarzbaum PJ.** A volume regulatory response can be triggered by nucleosides in human erythrocytes, a perfect osmometer no longer. *J Biol Chem* 285: 6134–6144, 2010.
49. **Pafundo DE, Chara O, Faillace MP, Krumschnabel G, Schwarzbaum PJ.** Kinetics of ATP release and cell volume regulation of hyposmotically challenged goldfish hepatocytes. *Am J Physiol Regul Integr Comp Physiol* 294: R220–R233, 2008.
50. **Pafundo DE, Mut P, Pérez Recalde M, González-Lebrero RM, Fachino V, Krumschnabel G, Schwarzbaum PJ.** Effects of extracellular nucleotides and their hydrolysis products on regulatory volume decrease of trout hepatocytes. *Am J Physiol Regul Integr Comp Physiol* 287: R833–R843, 2004.
51. **Pedersen S, Pedersen SF, Nilius B, Lambert IH, Hoffmann EK.** Mechanical stress induces release of ATP from Ehrlich ascites tumor cells. *Biochim Biophys Acta* 1416: 271–284, 1999.
52. **Robson SC, Sévigny J, Zimmerman H.** The ENTPDase family of ectonucleotidases: structure function relationships, and pathophysiological significance. *Purinergic Signal* 2: 409–430, 2006.
53. **Roman RM, Lomri N, Braunstein G, Feranchak AP, Simeoni LA, Davison AK, Mechetner E, Schwiebert EM, Fitz JG.** Evidence for multidrug resistance-1 P-glycoprotein-dependent regulation of cellular ATP permeability. *J Membr Biol* 183: 165–173, 2001.
54. **Sabirov RZ, Okada Y.** ATP-conducting maxi-anion channel: a new player in stress-sensory transduction. *Jpn J Physiol* 54: 7–14. 2004.
55. **Sauer H, Hescheler J, Wartenberg M.** Mechanical strain-induced Ca^{2+} waves are propagated via ATP release and purinergic receptor activation. *Am J Physiol Cell Physiol* 279: C295–C307, 2000.
56. **Schöfl C, Ponczek M, Mader T, Waring M, Benecke H, von zur Mühlen A., Mix H., Cornberg M., Böker KH, Manns MP, Wagner S.** Regulation of cytosolic free calcium concentration by extracellular nucleotides in human hepatocytes. *Am J Physiol Gastrointest Liver Physiol* 276: G164–G172, 1999.
57. **Schwarzbaum PJ, Frischmann ME, Krumschnabel G, Rossi RC, Wieser W.** Functional role of ecto-ATPase activity in goldfish hepatocytes. *Am J Physiol Regul Integr Comp Physiol* 274: R1031–R1038, 1998.
58. **Strehler BL.** Bioluminiscence assay: principles and practice. *Methods Biochem Anal* 16: 99–181, 1968.
59. **Wang Y, Roman R, Lidofsky SD, Fitz JG.** Autocrine signaling through ATP release represents a novel mechanism for cell volume regulation. *Proc Natl Acad Sci USA* 93: 12020–12025, 1996.
60. **Wood E, Broekman MJ, Kirley TL, Diani-Moore S, Tickner M, Drosopoulos JH, Islam N, Park JI, Marcus AJ, Rifkind AB.** Cell-type specificity of ectonucleotidase expression and upregulation by 2,3,7,8-tetrachlorodibenzo-p-dioxin. *Arch Biochem Biophys* 407: 49–62, 2002.
61. **Zhang Luo L FL, Gustafson E, Palmer K, Qiao X, Fan X, Yang S, Laz TM, Bayne M, Monsma F.** P2Y13: identification and characterization of a novel Galphai-coupled ADP receptor from human and mouse. *J Pharmacol Exp Ther* 301: 705–713, 2002.
62. **Zimmermann H, Zebisch M, Sträter N.** Cellular function and molecular structure of ecto-nucleotidases. *Purinergic Signal* 8: 437–502, 2012.